Structural and Mössbauer analyses of ultrafine $Sr_{1-x}La_xFe_{12-x}Zn_xO_{19}$ and $Sr_{1-x}La_xFe_{12-x}Co_xO_{19}$ hexagonal ferrites synthesized by chemical co-precipitation

2004 J. Phys.: Condens. Matter 16 5359

(http://iopscience.iop.org/0953-8984/16/29/025)

INSTITUTE OF PHYSICS PUBLISHING JOURNAL OF PHYSICS: CONDENSED MATTER

J. Phys.: Condens. Matter **16** (2004) 5359–5376 PII: S0953-8984(04)77409-3

Structural and Mössbauer analyses of ultrafine $Sr_{1-x}La_xFe_{12-x}Zn_xO_{19}$ and $Sr_{1-x}La_xFe_{12-x}Co_xO_{19}$ hexagonal ferrites synthesized by chemical co-precipitation

L Lechevallier[1,2,4], J M Le Breton[2], J F Wang[3] and I R Harris[3]

[1] Laboratoire de Physique des Matériaux et des Surfaces, Université de Cergy Pontoise, 95031 Cergy Pontoise, France
[2] Groupe de Physique des Matériaux, UMR CNRS 6634, Université de Rouen, 76801 Saint Etienne du Rouvray, France
[3] School of Metallurgy and Materials, The University of Birmingham, Edgbaston, Birmingham B15 2TT, UK

E-mail: Luc.Lechevallier@univ-rouen.fr

Received 5 March 2004
Published 9 July 2004
Online at stacks.iop.org/JPhysCM/16/5359
doi:10.1088/0953-8984/16/29/025

Abstract

Ultrafine M-type hexagonal ferrites of nominal composition $Sr_{1-x}La_xFe_{12-x}Zn_xO_{19}$ and $Sr_{1-x}La_xFe_{12-x}Co_xO_{19}$ with $x = 0$, 0.1, 0.2, 0.3 and 0.4 were produced by chemical co-precipitation. The phase make-up of the samples was investigated by x-ray diffraction. The analyses show that the hexagonal M-type phase is the main phase in all the samples. Secondary (La, Sr)FeO_3, $ZnFe_2O_4$ and $CoFe_2O_4$ phases are also detected, indicating that the La, Zn and Co content in the M-type phase is lower than the nominal content.

A complete Mössbauer analysis of the substitution effects in the M-type phase was made. The results show that the M-type phase contains La^{3+} in the same proportion as Zn^{2+} and La^{3+} in the same proportion as Co^{2+}, in the La–Zn and La–Co samples, respectively. The evolution with x of the hyperfine parameters of the components used to fit the contribution of the M-type phase have been interpreted consistently in relation to the substitution effects by means of the comparison between the spectra of the La–Zn and La–Co substituted samples. The results show unambiguously that La^{3+} ions are located in the Sr^{2+} sites, Zn^{2+} ions are located in the $4f_1$ sites and Co^{2+} ions are located in both $4f_2$ and 2a sites.

[4] Address for correspondence: Groupe de Physique des Materiaux, UMR 6634 CNRS, Université de Rouen, Site Universitaire du Madrillet, avenue de l'Université-BP 12, 76801 Saint Etienne du Rouvray Cedex, France.

1. Introduction

Since the discovery of the M-type $BaFe_{12}O_{19}$ and $SrFe_{12}O_{19}$ hexagonal ferrites, and because of the large volume of the market share that they still represent, in the last ten years numerous studies have been made to improve their magnetic properties. Because the magnetic moments are carried by the Fe^{3+} ions, the magnetic properties of the M-type $SrFe_{12}O_{19}$ hexagonal ferrites can be changed by substituting some Fe^{3+} ions by other ions. If Fe^{3+} is substituted by a divalent ion (Zn^{2+} or Co^{2+}), it is necessary to substitute simultaneously Sr^{2+} by a trivalent ion (La^{3+}) in order to compensate for the excess of negative charge. Compared to $SrFe_{12}O_{19}$, a $Sr_{0.7}La_{0.3}Fe_{11.7}Zn_{0.3}O_{19}$ ferrite shows a slight increase (4%) of the saturation magnetization, but an important decrease (10%) of the K_1 anisotropy constant [1]. On the other hand, the La–Co substitution leads to a significant improvement of the magnetic properties of the M-type phase [2–5]. For example, a large increase of the coercivity (25%) and a slight increase of the remanence (3%) are observed at room temperature in $Sr_{0.8}La_{0.2}Fe_{11.8}Co_{0.2}O_{19}$ ferrites as compared to $SrFe_{12}O_{19}$ ferrites [5]. This improvement is largely associated with the increase of both magneto-crystalline anisotropy and saturation magnetization. The intrinsic magnetic properties (anisotropy field, saturation magnetization) being strongly dependent on the atomic magnetism, the investigation of the sublattice occupation of Zn^{2+} and Co^{2+} ions in the M-type-hexagonal crystal, and the effects of these substitutions on the other Fe^{3+} sites are thus essential for the fundamental understanding of these effects.

M-type ferrites crystallize in an hexagonal structure with 64 ions per unit cell on 11 different symmetry sites ($P6_3/mmc$ space group). The 24 Fe^{3+} atoms are distributed over five distinct sites: three octahedral sites (12k, 2a and $4f_2$), one tetrahedral site ($4f_1$) and one bipyramidal site (2b). The magnetic structure is ferrimagnetic with five different sublattices: three parallel (12k, 2a and 2b) and two antiparallel ($4f_1$ and $4f_2$) [6].

The distribution of Zn^{2+} in $BaFe_{12-2x}Zn_xTi_xO_{19}$ ferrites was investigated by Mössbauer spectrometry [7]. It has been shown that Zn^{2+} is substituted for Fe^{3+} in the tetrahedral $4f_1$ site of the M-type structure, in agreement with the fact that in spinels, the Zn^{2+} ion has a marked preference for tetrahedral sites [8, 9]. As the corresponding magnetic sublattice is antiparallel, this substitution leads to an increase of the saturation magnetization [1].

The cationic distribution of Co^{2+} in the M-type structure was recently investigated in $Sr_{1-x}La_xFe_{12-x}Co_xO_{19}$ hexagonal ferrites prepared by a ceramic process. Neutron diffraction analyses [10] have suggested that the Co^{2+} ions could be present in $4f_1$ sites, in agreement with the fact that large bivalent cations such as Co^{2+} are known to stabilize the spinel block structure and are often found on the spinel tetrahedral site [11]. However, Mössbauer spectrometry [12, 13], Raman spectroscopy [12] and nuclear magnetic resonance [14] have shown that Co^{2+} ions have a marked preference for octahedral sites, being substituted for Fe^{3+} in both $4f_2$ and 2a sites. The fact that Co^{2+} is present in both parallel (2a) and antiparallel ($4f_2$) magnetic sites explains the fact that the saturation magnetization does not vary significantly with x, in agreement with magnetization measurements [4, 5].

A further increase of the magnetic performance of M-type ferrites could be achieved by decreasing the particle size. Such a decrease can be obtained by using chemical synthesis methods (hydrothermal synthesis [15] or co-precipitation [16]). With the chemical co-precipitation process, ultrafine single domain M-type $SrFe_{12}O_{19}$ hexagonal ferrite particles, with narrow particle size distribution, can be obtained that are suitable for application in microelectro-mechanical systems (micro-sized motors, actuators, mini pumps, etc). For such applications, the particles are required to be chemically homogeneous.

We used the chemical co-precipitation process to synthesize $Sr_{1-x}La_xFe_{12-x}Zn_xO_{19}$ and $Sr_{1-x}La_xFe_{12-x}Co_xO_{19}$ M-type ferrites. With the aim of characterizing the structure

of these co-precipitated powders, x-ray diffraction and Mössbauer spectrometry analyses were undertaken. The Mössbauer spectrometry was used particularly to study the cationic distribution of Zn^{2+} and Co^{2+} in the M-type structure of the co-precipitated powders. By comparing the spectra of the La–Zn and La–Co substituted samples, a complete Mössbauer analysis of the substitution effects in the M-type phase was possible. The results are presented here, discussed and compared to the results obtained for La–Zn and La–Co substituted M-type ferrites prepared by the conventional ceramic process.

2. Experimental details

Two series of $Sr_{1-x}La_xFe_{12-x}Zn_xO_{19}$ and $Sr_{1-x}La_xFe_{12-x}Co_xO_{19}$ powders (namely La–Zn and La–Co powders) with different substitution ratios ($x = 0, 0.1, 0.2, 0.3, 0.4$) were prepared according to a chemical co-precipitation process.

The chemical precursors used to prepare the powders were $Fe(NO_3)_3{\cdot}9H_2O$, $Sr(NO_3)_2$, $La(NO_3)_3{\cdot}nH_2O$, $M(NO_3)_2$ (M = Zn or Co) and NaOH. The precursors were weighed according to different values of x, where x was varied between 0 and 0.4, while $[Sr^{2+} + La^{3+}]/[Fe^{3+} + M^{2+}]$ and $[NO_3^-]/[OH^-]$ ratios were fixed at $1/8$ and $1/2$, respectively. A water solution containing Sr^{2+}, Fe^{3+} and dopants La^{3+}, M^{2+} was poured into the solution of NaOH.

Aqueous suspensions containing the precipitated products were stirred at 1000 rpm and heated to 100 °C for 2 h in an autoclave. The co-precipitates were carefully washed and vacuum filtered using deionized water, and then dried at 80 °C overnight. Because of the agglomeration of the dry co-precipitates, they were hand-crushed with a mortar and pestle before calcination was conducted at 1000 °C for 2 h in air to produce La–Co substituted SrM fine particles.

X-ray diffraction analysis was performed by reflection with a Siemens D5000 system in Bragg–Brentano θ–2θ geometry. The x-ray generator was equipped with a Co anticathode, using Co Kα radiation ($\lambda = 0.179\,09$ nm).

A Mössbauer spectrometry analysis was performed at room temperature in transmission geometry using a ^{57}Co source in a rhodium matrix. The isomer shift (relative to metallic α-Fe at room temperature), quadrupolar shift and hyperfine field are denoted δ, ε and B, respectively. Estimated errors for the hyperfine parameters originate from the statistical errors σ given by the fitting program [17], taking 3σ.

3. Results

3.1. Structural investigation and phase analysis

3.1.1. X-ray diffraction. The x-ray diffraction patterns of the powders are shown in figure 1 for the La–Zn substituted ferrites and in figure 2 for the La–Co substituted ferrites. In each pattern, all the peaks of the hexagonal M-type phase are observed, indicating that this phase is the main constituent in all the samples. However, as diffraction peaks corresponding to secondary phases are observed, the samples are not in the single phase condition.

In the patterns of the $x = 0$ powders, two extra peaks with weak intensities are observed at $2\theta = 38.2°$ and 54.0°, which correspond to the $Sr_7Fe_{10}O_{22}$ phase (JCPDS file 22-1427).

For the La–Zn samples, the peaks of the $Sr_7Fe_{10}O_{22}$ phase are not observed, and new peaks are present, with an intensity that increases with the substitution concentration x. These peaks correspond to the (La, Sr)FeO_3 type phase. As x increases, the peaks shift towards low angles, indicating that the composition of the (La, Sr)FeO_3 phase changes, being $La_{0.5}Sr_{0.5}FeO_3$ (JCPDS file 82-1962) for $x = 0.2$ and $La_{0.8}Sr_{0.2}FeO_3$ (JCPDS file 35-1480) for $x = 0.4$. It should be noted that the La content of this phase increases with the substitution concentration. For the $x = 0.2$ and 0.4 samples, other peaks appear with a weak intensity, the most intense one

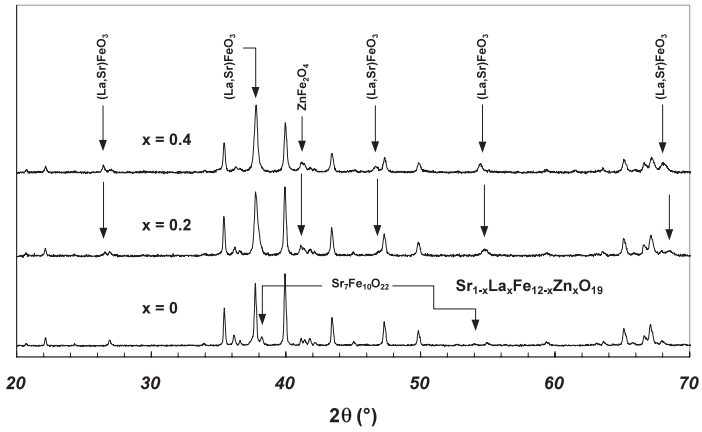

Figure 1. X-ray diffraction patterns of some $Sr_{1-x}La_xFe_{12-x}Zn_xO_{19}$ powders. Only the main peak of the $ZnFe_2O_4$ phase is visible in the $x = 0.2$ and 0.4 patterns (the intensity of the other peaks being too weak for these peaks to be observable). The non-indexed peaks are those of the M-type phase.

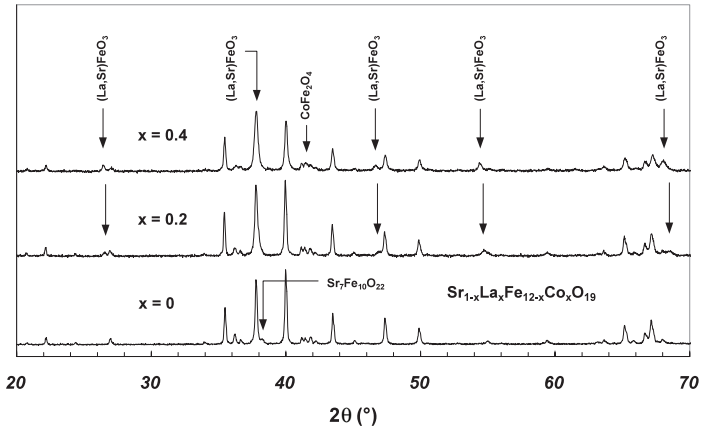

Figure 2. X-ray diffraction patterns of the $Sr_{1-x}La_xFe_{12-x}Co_xO_{19}$ powders. Only the main peak of the $CoFe_2O_4$ phase is visible in the $x = 0.4$ pattern (the intensity of the other peaks being too weak for these peaks to be observable). The non-indexed peaks are those of the M-type phase.

being observed at $2\theta = 41.2°$. These peaks are characteristic of the $ZnFe_2O_4$ phase (JCPDS file 82-1049).

The x-ray diffraction patterns of the La–Co samples show similar variations to those of the La–Zn samples. Extra peaks are clearly observed, with an intensity that increases with x and which correspond to the (La, Sr)FeO_3 type phase. We also observe that the La content of this phase increases with x. For the $x = 0.4$ sample other peaks appear, the most intense one being observed at $2\theta = 41.5°$. These peaks are characteristic of the $CoFe_2O_4$ phase (JCPDS file 79-1744).

These results show that when La, Zn and Co are introduced in the powders, (La, Sr)FeO_3, $ZnFe_2O_4$ and $CoFe_2O_4$ secondary phases are formed, with a proportion that increases with the substitution concentration. This indicates that some La, Zn and Co atoms do not enter the M-type hexaferrite phase. So the La, Zn and Co content in the M-type phase is lower than that indicated by the nominal values.

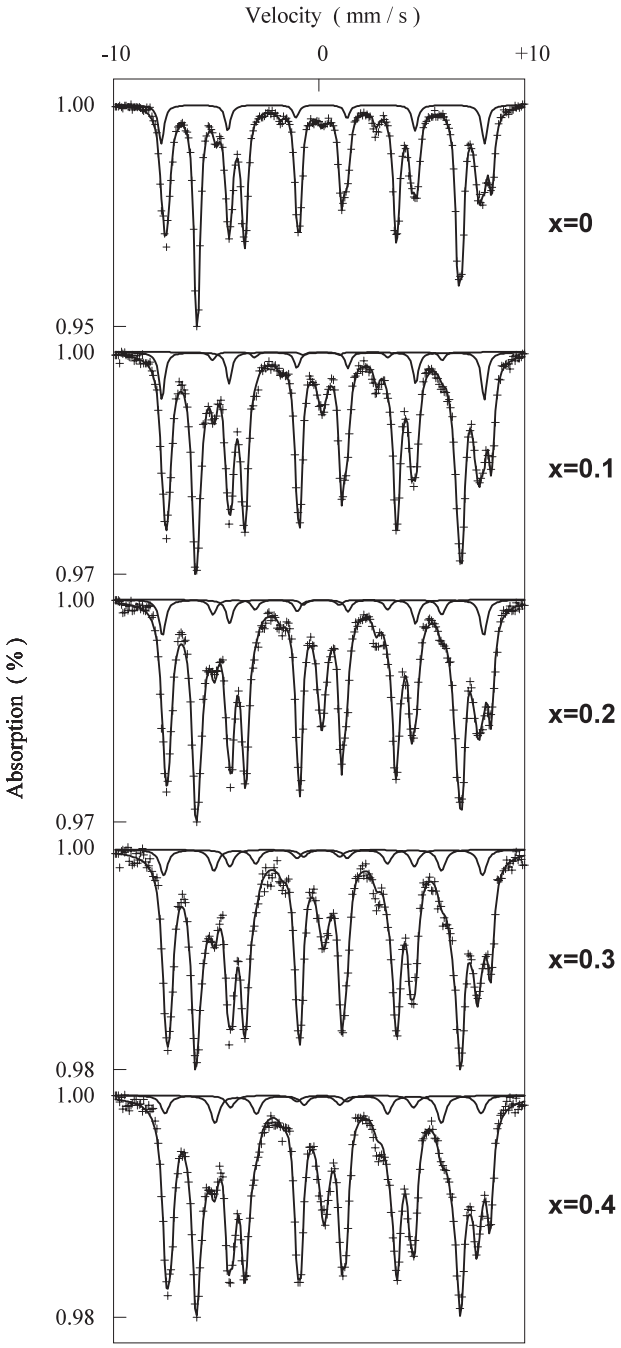

Figure 3. Room temperature Mössbauer spectra of the $Sr_{1-x}La_xFe_{12-x}Zn_xO_{19}$ powders for the indicated compositions. Both 2a(Fe) and 2a(Zn) contributions (see the text) are displayed.

3.1.2. Mössbauer spectrometry. The room temperature Mössbauer spectra of the La–Zn and La–Co powders are shown in figures 3 and 4, respectively. Both series of spectra were fitted according to the results of the x-ray diffraction analysis. The contribution of the

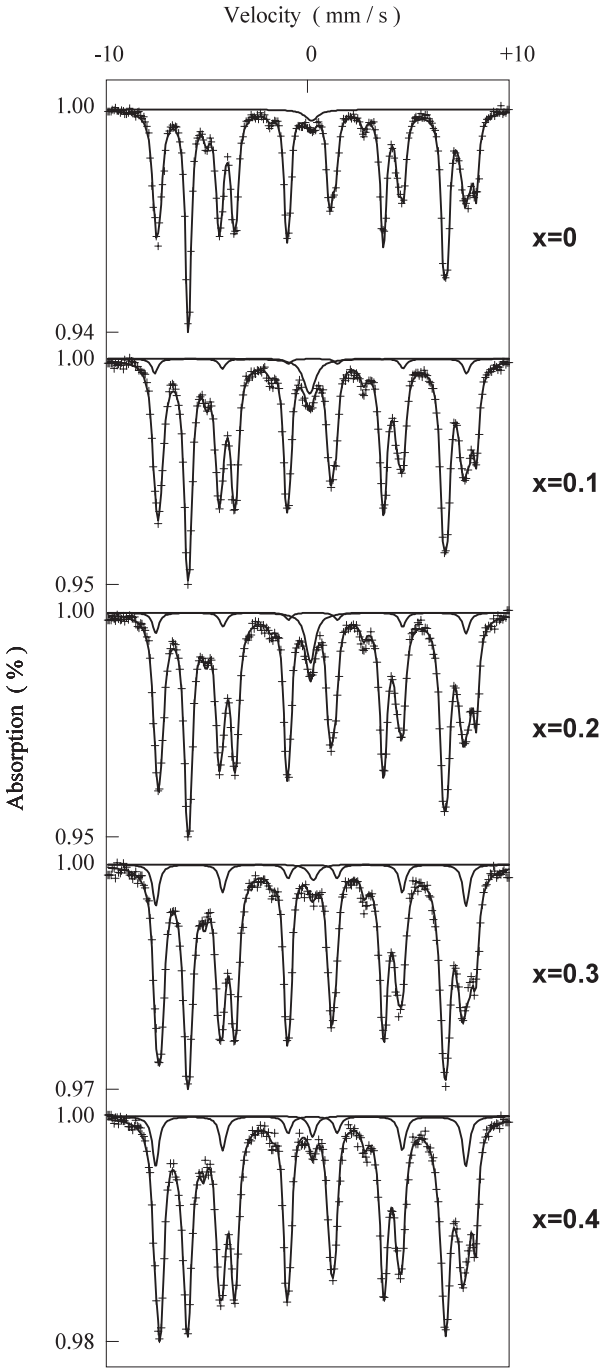

Figure 4. Room temperature Mössbauer spectra of the $Sr_{1-x}La_xFe_{12-x}Co_xO_{19}$ powders for the indicated compositions. The paramagnetic and magnetic contributions of the secondary phases (see the text) are displayed.

M-type phase was fitted by taking into account the presence of the Zn^{2+} and Co^{2+} ions in the crystal structure, according to a model that is described in section 3.2. The contribution of

the $Sr_7Fe_{10}O_{22}$ phase was fitted in the spectra of the $x = 0$ samples by a paramagnetic singlet ($\delta = 0.34 \pm 0.03$ mm s^{-1}), as in [18].

The room temperature Mössbauer contribution of the (La, Sr)FeO_3 phase depends on the La content: for a low La content (composition close to $SrFeO_3$) the contribution is paramagnetic [19], while for a high La content (composition close to $LaFeO_3$) the contribution is magnetic [20]. For intermediate compositions, the room temperature contribution consists of a paramagnetic singlet and of a magnetic sextet, as for the (Gd, Sr)FeO_3 phase [19]. The room temperature hyperfine parameters of the sextet are close to those of the $LaFeO_3$ phase ($\delta = 0.28 \pm 0.01$ mm s^{-1}, $2\varepsilon = -0.02 \pm 0.03$ mm s^{-1}, $B = 52.1 \pm 0.2$ T [20]).

As the $ZnFe_2O_4$ phase is paramagnetic at room temperature [21, 22], its contribution consists of a paramagnetic singlet, with $\delta = 0.27 \pm 0.06$ mm s^{-1}.

The room temperature Mössbauer contribution of the $CoFe_2O_4$ phase is magnetic, consisting of two sextets that correspond to the tetrahedral (A) and octahedal (B) Fe sites of the $CoFe_2O_4$ structure. Annealed $CoFe_2O_4$ nanocrystalline particles are magnetically ordered at room temperature and the values of the room temperature hyperfine parameters depend on the preparation method, the particle size and the annealing temperature, being $\delta = 0.16$ to 0.40 mm s^{-1}, $2\varepsilon = -0.02$ to 0.01 mm s^{-1}, $B = 50.5$ to 51.3 T for the A site, and $\delta = 0.27$ to 0.51 mm s^{-1}, $2\varepsilon = -0.03$ to 0.04 mm s^{-1}, $B = 52.7$ to 54.3 T for the B site [23, 24].

As shown by x-ray diffraction analysis, the secondary (La, Sr)FeO_3, $ZnFe_2O_4$ and $CoFe_2O_4$ phases are present in low proportions in the La–Zn and La–Co substituted powders. Thus, for both series of spectra, we fitted the contributions of the secondary phases by using one magnetic component and one paramagnetic component. For the La–Zn series, the magnetic component (hyperfine parameters: $\delta = 0.29 \pm 0.03$ mm s^{-1}, $2\varepsilon = -0.10 \pm 0.03$ mm s^{-1}, $B = 50.1 \pm 0.2$ T) corresponds to the magnetic component of (La, Sr)FeO_3, and the paramagnetic component (singlet with $\delta = 0.27 \pm 0.06$ mm s^{-1}) corresponds both to $ZnFe_2O_4$ and to the paramagnetic component of (La, Sr)FeO_3. For the La–Co series, the magnetic component (hyperfine parameters: $\delta = 0.29 \pm 0.03$ mm s^{-1}, $2\varepsilon = -0.10 \pm 0.03$ mm s^{-1}, $B = 50.2 \pm 0.2$ T) corresponds both to $CoFe_2O_4$ and to the magnetic component of (La, Sr)FeO_3 (the hyperfine fields of these two contributions being very close) and the paramagnetic component (singlet with $\delta = 0.27 \pm 0.10$ mm s^{-1}) corresponds to the paramagnetic component of (La, Sr)FeO_3. The contributions of the secondary phases are shown in the spectra of the La–Co samples (figure 4).

The evolution of the relative intensity of the contributions of the secondary phases is reported in figure 5 for La–Zn samples and in figure 6 for the La–Co samples. For La–Zn samples, the increase of the relative intensity of both magnetic and paramagnetic contributions indicates that the proportion of the (La, Sr)FeO_3 and $ZnFe_2O_4$ phases increases with x. For the La–Co samples, the intensity of the paramagnetic component first increases, in agreement with the increase of the proportion of the (La, Sr)FeO_3 phase in the sample, and then decreases for x higher than 0.2 due to the fact that the La content in the (La, Sr)FeO_3 phase increases. An increase of the La content leads both to a decrease of the intensity of the paramagnetic component of the (La, Sr)FeO_3 phase and to an increase in the intensity of the magnetic component. For each sample, the relative intensity of all the secondary phases does not exceed 10% of the whole Mössbauer intensity.

3.2. Investigation of the M-type phase: substitution effects

The investigation of the substitution effects in the M-type phase is made by Mössbauer spectrometry. Usually, the Mössbauer contribution of the M-type phase is fitted with five components that correspond to the five different sites of the M-type crystal structure, i.e. the 12k, $4f_1$, $4f_2$, 2a and 2b sites [25].

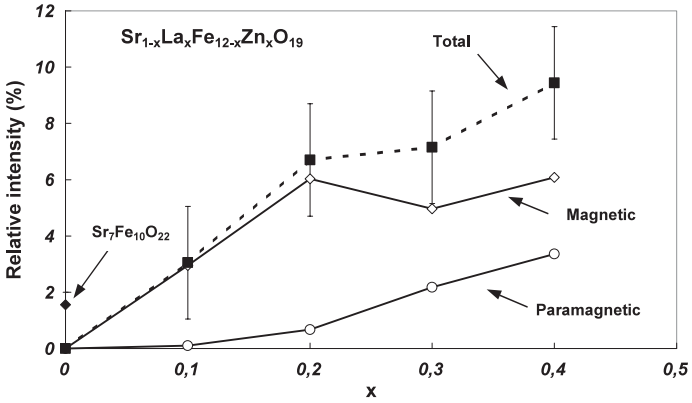

Figure 5. Composition dependence of the Mössbauer relative intensity (%) of the contributions of the secondary phases in the $Sr_{1-x}La_xFe_{12-x}Zn_xO_{19}$ spectra. The contribution of the $Sr_7Fe_{10}O_{22}$ paramagnetic phase is fitted in the $x = 0$ spectrum only. The 'magnetic' curve refers to (La, Sr)FeO_3, and the 'paramagnetic' curve refers to both (La, Sr)FeO_3 and $ZnFe_2O_4$ (see the text). The 'total' curve refers to the total intensity of the (La, Sr)FeO_3 and $ZnFe_2O_4$ contributions.

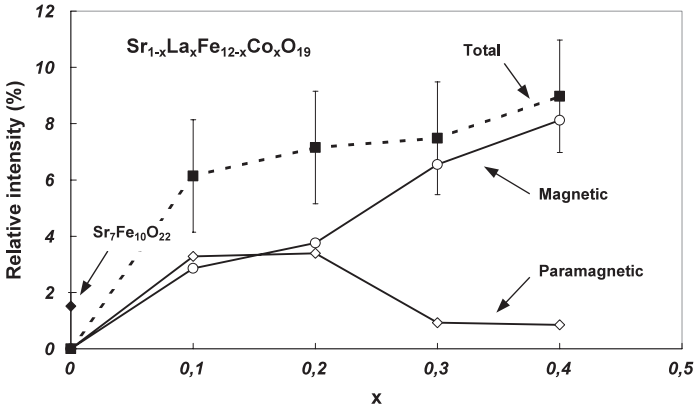

Figure 6. Composition dependence of the Mössbauer relative intensity (%) of the contributions of the secondary phases in the $Sr_{1-x}La_xFe_{12-x}Co_xO_{19}$ spectra. The contribution of the $Sr_7Fe_{10}O_{22}$ paramagnetic phase is fitted in the $x = 0$ spectrum only. The 'magnetic' curve refers to (La, Sr)FeO_3 and $CoFe_2O_4$ and the 'paramagnetic' curve refers to both (La, Sr)FeO_3 (see the text). The 'total' curve refers to the total intensity of the (La, Sr)FeO_3 and $CoFe_2O_4$ contributions.

The room temperature Mössbauer spectrum of the $x = 0$ sample of the La–Co series is shown in figure 7. In this spectrum, the two most intense peaks are the peaks 1 and 6 of the 12k sextet. These peaks should thus have the same width and the same intensity. This is clearly not the case here. Such an 'anomaly' could be due to stacking faults of the R and S blocks of the M-type structure, possibly associated with the co-precipitation process used to prepare the powders. It must be mentioned that the Mössbauer spectra of powders prepared by hydrothermal synthesis or by a conventional ceramic process do not show this 'anomaly' [12, 13, 18]. We made preliminary fittings by replacing the 12k sextet by six singlets in order to determine the evolution of the full width at half maximum (fwhm) of these two peaks with the substitution rate, for both the La–Zn and La–Co series. The observed values are reported in figures 8(a) (La–Zn) and (b) (La–Co). The evolution is the same for the two series

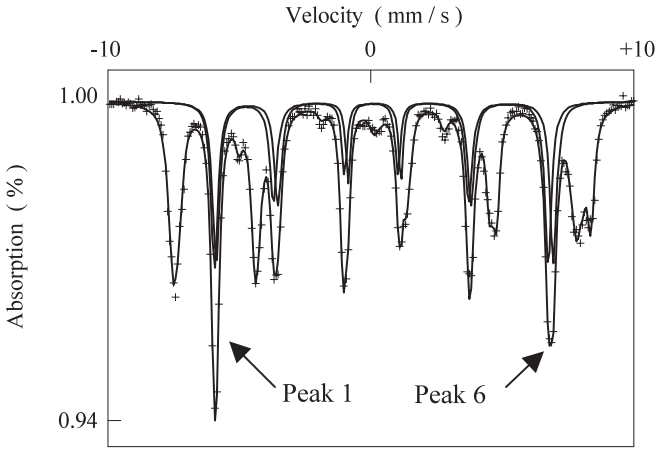

Figure 7. Room temperature Mössbauer spectra of a $SrFe_{12}O_{19}$ powder ($x = 0$, La–Co series). The two contributions of the 12k site are displayed on the spectrum.

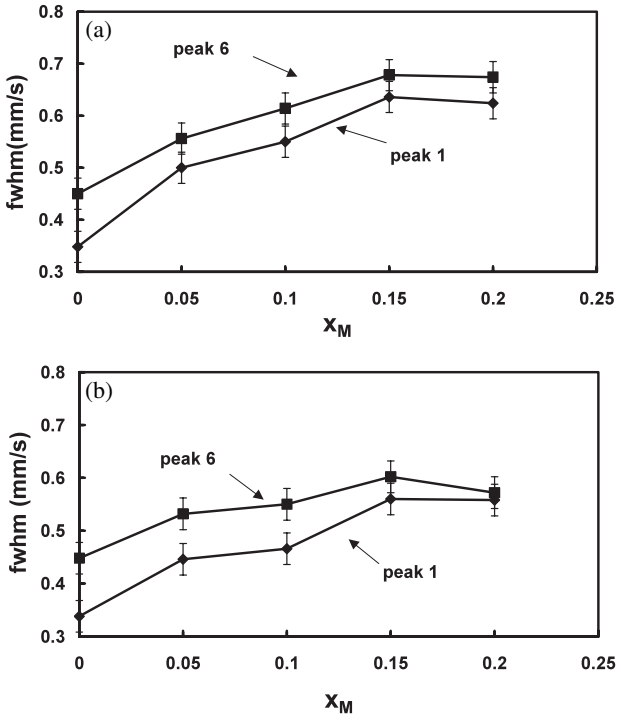

Figure 8. Full width at half maximum (fwhm) for the peaks 1 and 6 of the Mössbauer contribution of the 12k site, as a function of the effective La–Zn (a) and La–Co (b) content in the M-type phase x_M.

of powders. As x increases, the fwhm of the two peaks increases, due to substitution effects, as in the case of Al^{3+}/Fe^{3+} [26] or Co^{2+}/Fe^{3+} [13] substitutions, and the difference between the two values decreases. The fact that the difference between the fwhm values of the two peaks decreases as x increases could be due to the fact that the effect of the stacking faults is masked by the substitution effects. Consequently, we fitted the contribution of the 12k site using two

Table 1. Mössbauer hyperfine parameters at room temperature and relative proportion of the 2a(Zn) contribution (relative to the total Mössbauer intensity of the 2a contribution) for each La–Zn sample. δ is relative to metallic iron. Estimated errors are ± 0.03 mm s^{-1} for δ, ± 0.05 mm s^{-1} for 2ε, ± 0.5 T for B.

x_M	0	0.05	0.1	0.15	0.2
Proportion (%)	0	15	30	45	60
δ (mm s^{-1})	—	0.34	0.35	0.36	0.38
2ε (mm s^{-1})	—	0.32	0.31	0.31	0.32
B (T)	—	36.3	36.2	36.0	35.8

sextets. These two sextets have different hyperfine parameters, and the same relative intensity. In the following, the hyperfine parameters of the 12k contribution for both La–Zn and La–Co substituted samples are the mean values of the two sextets.

The preliminary fittings revealed that the relative intensities deviate from the crystallographic occupancy, and for the spectra of the unsubstituted samples the proportions 12:4:4:2:1.2 for the 12k, $4f_1$, $4f_2$, 2a and 2b sites, respectively, were used. Such a deviation is generally observed in the M-type hexaferrites, and can be attributed to anisotropic f-factors, to stacking faults [27], or to the pronounced anisotropy of the 2b site [28].

3.2.1. La–Zn samples. As La and Zn containing secondary phases are present in the substituted samples, the La and Zn content in the M-type phase is lower than that corresponding to the nominal content. According to the Mössbauer relative intensities of the secondary phases deduced from the fittings, we have considered that the La and Zn content in the M-type phase (x_M) is half the nominal value (x). So, for $x = 0.1, 0.2, 0.3, 0.4$, we considered $x_M = 0.05$, 0.1, 0.15, 0.2.

As x increases, we observe on the Mössbauer spectra the appearance of two extra absorption lines at about 6 and -6 mm s^{-1}, respectively, with increasing intensities (figure 3). These two extra lines, which are not observed in the spectra of the La–Co samples, are attributed to one magnetic component (sextet). The fitted hyperfine parameters of this component are given in table 1. The isomer shift (0.2–0.3 mm s^{-1}) corresponds to Fe^{3+}, showing that it cannot correspond to the contribution of Fe^{2+} ions. On the other hand, this component does not correspond to any of the secondary phases detected by x-ray diffraction analysis. In order to confirm its presence, we investigated a $Sr_{0.7}La_{0.3}Fe_{11.7}Zn_{0.3}O_{19}$ powder prepared by a ceramic process. The corresponding Mössbauer spectrum, shown in figure 9, reveals the same extra lines (at about 6 and -6 mm s^{-1}), which are attributed to a sextet, the corresponding hyperfine parameters being $\delta = 0.43 \pm 0.03$ mm s^{-1}, $2\varepsilon = 0.37 \pm 0.05$ mm s^{-1} and $B = 36.4 \pm 0.5$ T. These values are similar to those of the extra component fitted in the spectra of the co-precipitated samples. As revealed by XRD analysis (not shown here), the La–Zn substituted ceramic sample contains no (La, Sr)FeO_3 and only traces of $ZnFe_2O_4$. This confirms that the extra component does not correspond to one of the secondary phases. Consequently, this extra component is attributed to the M-type phase, and is related to the presence of the Zn^{2+} ions.

It is known that the Zn^{2+} ion has a strong preference for tetrahedral sites and therefore for the $4f_1$ site of the M type structure [8, 9]. Consequently, the spectra of the La–Zn substituted samples were fitted assuming a distribution of Zn^{2+} in $4f_1$ sites. As the $4f_1$ site is in the close vicinity of the 2a site, this site is perturbed by the Zn^{2+}/Fe^{3+} substitution. In this case, the substitution of one Fe^{3+} ion by one Zn^{2+} ion (which is non-magnetic) in a $4f_1$ site induces a perturbation of the 2a site, and the Mössbauer contribution of the 2a site has different hyperfine parameters from the non-perturbed 2a site. Consequently, the contribution of the 2a site in the

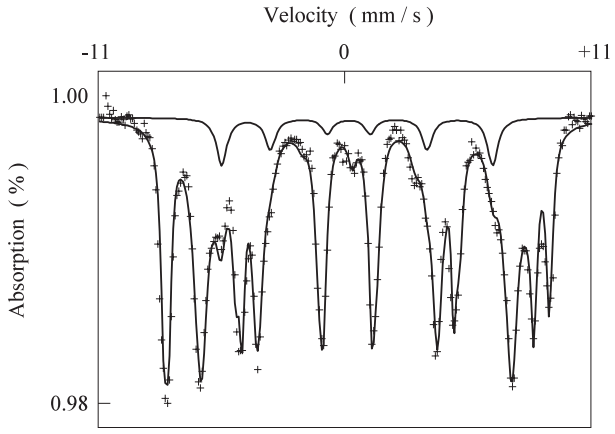

Figure 9. Room temperature Mössbauer spectrum of a $Sr_{0.7}La_{0.3}Fe_{11.7}Co_{0.3}O_{19}$ ($x = 0.4$) powder prepared by a conventional ceramic process. The 2a(Zn) contribution (see the text) is displayed.

Mössbauer spectra is fitted with two sextets: one for the non-perturbed site, namely 2a(Fe), and one for the perturbed site, namely 2a(Zn). The 2a(Zn) contribution thus corresponds to the extra component discussed in the previous paragraph. As the Zn^{2+} ion is non-magnetic, the hyperfine field of the 2a(Zn) contribution must be lower than that of the 2a(Fe) contribution. As a $4f_1$ site is surrounded by three 2a sites (see figure 10), the substitution of one Fe^{3+} ion by a non-magnetic Zn^{2+} ion in the $4f_1$ site induces an increase of the relative intensity of the 2a(Zn) component and a decrease of the relative intensity of the 2a(Fe) component, proportionally to the substitution concentration x. The 2a(Fe) and 2a(Zn) contributions are displayed on each spectrum in figure 3. The proportions of the 2a(Fe) and 2a(Zn) components of the 2a contribution were calculated to be 85% and 15%, 70% and 30%, 55% and 45%, 40% and 60% for $x_M = 0.05, 0.1, 0.15, 0.2$, respectively.

The Mössbauer spectrum of the M-type phase in the La–Zn samples is thus fitted with seven components: 12k (two components), $4f_1$, $4f_2$, 2a(Fe), 2a(Zn) and 2b. The Mössbauer relative intensities of the seven components are fixed for all the samples to the values calculated by considering that the Zn^{2+} ions occupy the $4f_1$ site only. This leads to very satisfactory fittings of the La–Zn spectra, as shown in figure 3.

3.2.2. La–Co samples. As for the La–Zn samples, because La- and Co-containing secondary phases are present in the La–Co substituted samples, the La and Co content in the M type phase is lower than that corresponding to the nominal content. According to the Mössbauer relative intensities of the secondary phases deduced from the fittings, we have considered that the La and Co content in the M-type phase (x_M) is half the nominal value (x). Thus, for $x = 0.1, 0.2, 0.3, 0.4$, we considered $x_M = 0.05, 0.1, 0.15, 0.2$.

The Mössbauer investigation of La–Co ferrites synthesized by a ceramic process have shown that a valence change of some Fe^{3+} to Fe^{2+} occurs in the 2a site, consistent with the fact that the amount of La^{3+} in the M-type phase is higher than that of Co^{2+} [12]. Here, no Fe^{2+} contribution was observed in the La–Co spectra, indicating that both La^{3+} and Co^{2+} are present in the same proportions in the M-type phase.

As shown in La–Co substituted ferrites synthesized by a ceramic process, the Co^{2+} ions enter the M-type phase in the $4f_2$ and 2a sites [12, 13]. Preliminary fittings of the Mössbauer spectra of the co-precipitated powders confirmed this result, and showed that Co^{2+} is not

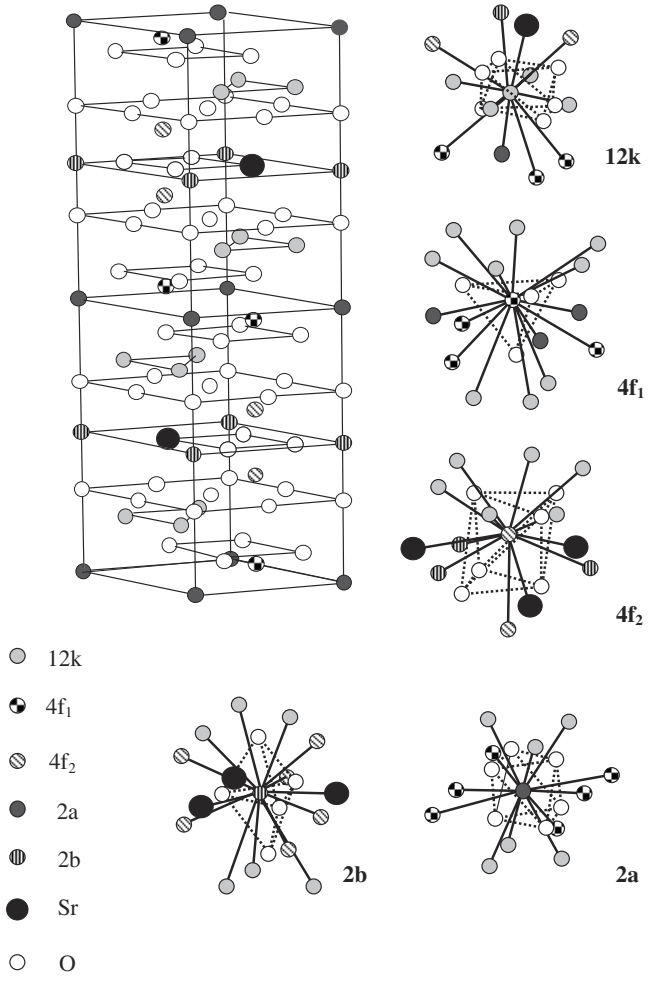

Figure 10. Crystal structure of the hexagonal M-type phase. The five Fe sites with their surroundings are displayed.

present in the $4f_1$ site. According to these observations, the spectra of the co-precipitated La–Co substituted samples were fitted assuming a distribution of Co^{2+} in $4f_2$ and 2a octahedral sites, with proportions that correspond to the relative proportions of these two sites in the M-type structure, namely $2/3$ and $1/3$.

The substitution of a Fe^{3+} ion by a Co^{2+} ion in a $4f_2$ site modifies the vicinity of the 2b site and the substitution of a Fe^{3+} ion by a Co^{2+} ion in a 2a site modifies the vicinity of the $4f_1$ site. However, because the Co^{2+} ion is magnetic, the 2b and $4f_1$ sites are only weakly perturbed by the Co^{2+}/Fe^{3+} substitution. Consequently, these substitutions do not require the use of extra contributions, as in the case of La–Zn samples.

The Mössbauer spectrum of the M-type phase in the La–Co samples is thus fitted with six components: 12k (two components), $4f_1$, $4f_2$, 2a and 2b. The Mössbauer relative intensities of the six components are fixed for all the samples to the values calculated by considering that the Co^{2+} ions occupy both $4f_2$ and 2a sites. This leads to very satisfactory fittings of the La–Co spectra, as shown in figure 4.

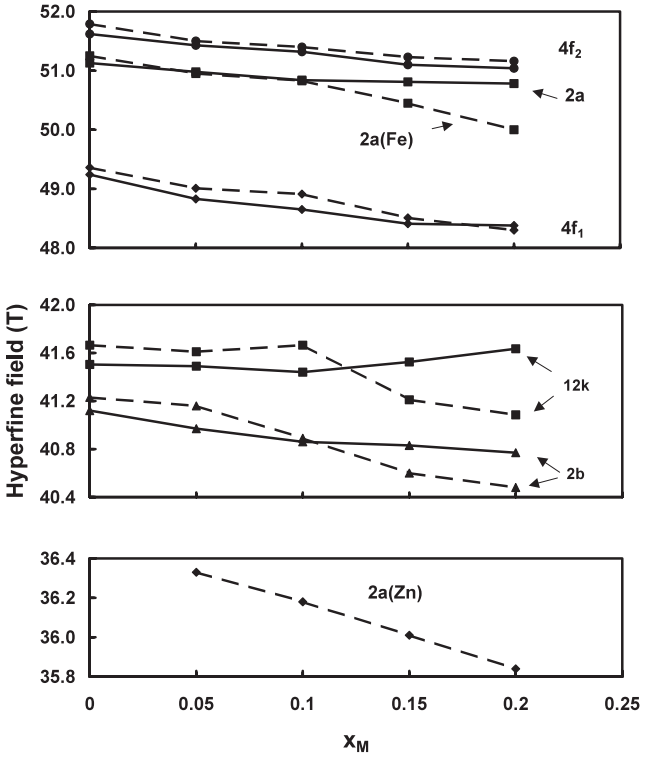

Figure 11. Hyperfine field of the different contributions used to fit the Mössbauer spectrum of the M-type phase. The continuous and dotted lines correspond to the La–Co and La–Zn powders, respectively. The experimental errors are ±0.1, ±0.2, ±0.2, ±0.3 and ±0.3 T, for the 12k, $4f_1$, $4f_2$, 2a and 2b contributions, respectively.

3.2.3. A comparison of the results. The fitted hyperfine parameters of the contributions to the Mössbauer spectra of the M-type phase in both La–Zn and La–Co substituted samples are reported as a function of x_M in figures 11–13.

In figure 11 the hyperfine fields of the 12k, $4f_1$, $4f_2$, 2a and 2b contributions are shown as a function of x_m. For both series of samples it can be observed that, as x_M increases, the hyperfine fields of the $4f_1$ and 2b contributions decrease significantly, while that of the $4f_2$ contribution decreases weakly. The differences between the La–Zn and La–Co samples arise from the 12k and 2a contributions. The hyperfine field of the 12k contribution decreases for the La–Zn samples, whereas it increases with x_M for the La–Co samples. On the other hand, the hyperfine field of the 2a contribution does not vary in the La–Co substituted samples, while those of both 2a(Fe) and 2a(Zn) contributions decrease significantly. These variations can be interpreted with respect to the presence of Zn^{2+} and Co^{2+} in the different sites of the M-type structure, and are discussed in section 3.2.4.

These variations lead to a decrease of the mean hyperfine field of the M-type phase in the La–Zn samples (from 45.5 ± 0.5 T for $x_M = 0$ down to 44.0 ± 0.5 for $x_M = 0.2$), in agreement with the substitution of magnetic Fe^{3+} ions by non-magnetic Zn^{2+} ions in the M-type structure. On the other hand, the mean hyperfine field of the M-type phase in La–Co samples remains constant when taking into account the experimental errors (45.4 ± 0.5 T for $x_M = 0$ and 45.1 ± 0.5 T for $x_M = 0.2$). This is attributed to the increase of the hyperfine field of the 12k contribution, which almost compensates for the decrease of the hyperfine fields at the $4f_1$,

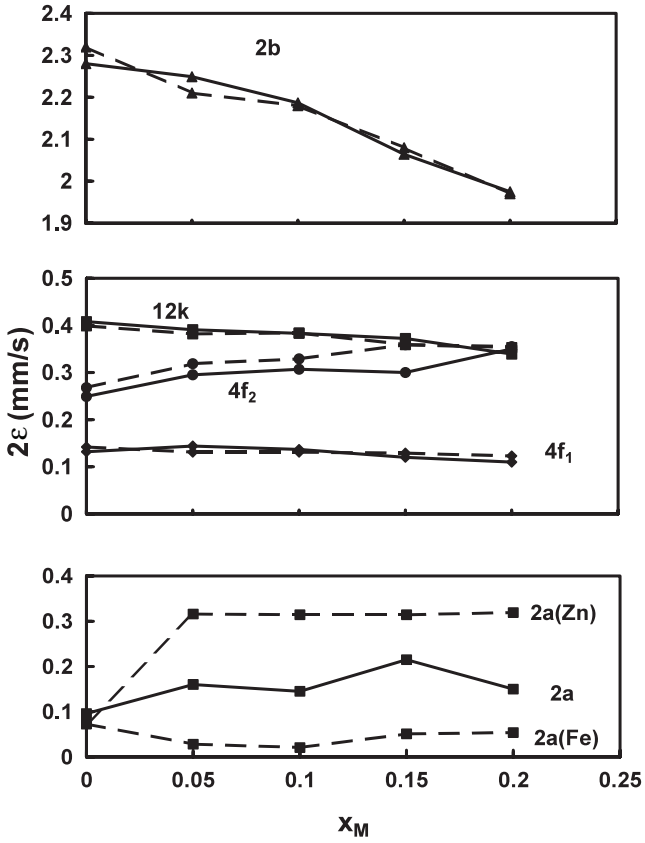

Figure 12. Quadrupolar shift of the different contributions used to fit the Mössbauer spectrum of the M-type phase. The continuous and dotted lines correspond to the La–Co and La–Zn powders, respectively. The experimental errors are ±0.02, ±0.04, ±0.04, ±0.09 and ±0.08 mm s^{-1}, for the 12k, $4f_1$, $4f_2$, 2a and 2b contributions, respectively.

$4f_2$ and 2b sites. These results indicate that the simultaneous substitution of Fe^{3+} for Co^{2+} in both $4f_2$ and 2a sites has a positive influence on the hyperfine field at the 12k site. Thus, the mean hyperfine field of the M-type phase does not decrease as x_M increases, contrary to the behaviour of the La–Zn substituted samples. This is in agreement with previous results obtained for ceramic $Sr_{1-x}La_xFe_{12-x}Co_xO_{19}$ [13] and $Sr_{1-x}La_xFe_{12-y}Co_yO_{19}$ [29] powders.

The variations of both the quadrupolar shift (figure 12) and isomer shift (figure 13) are similar to the corresponding variations obtained on La–Co ferrites prepared according to a ceramic process [13, 29]. It appears that the most striking features are, for both series of samples, a strong decrease of the quadrupolar shift of the 2b contribution, a slight increase of the quadrupolar shift of the $4f_2$ contribution, and a decrease of the isomer shift of the 2b contribution. On the other hand, a decrease of the isomer shift of the $4f_2$ contribution is observed for the La–Zn samples. These variations are attributed to the presence of La^{3+} in the vicinity of the 2b and $4f_2$ sites (figure 10), and are discussed in section 3.2.4.

The main difference between the behaviours of the two series of samples arises from the 2a site, as both quadrupolar and isomer shifts of the 2a(Fe) and 2a(Zn) contributions in the La–Zn spectra are much different from the values of the 2a contribution in the La–Co spectra. Thus, the vicinity of the 2a site appears to be strongly modified by the Fe^{3+}/Zn^{2+} substitution in the $4f_1$ site.

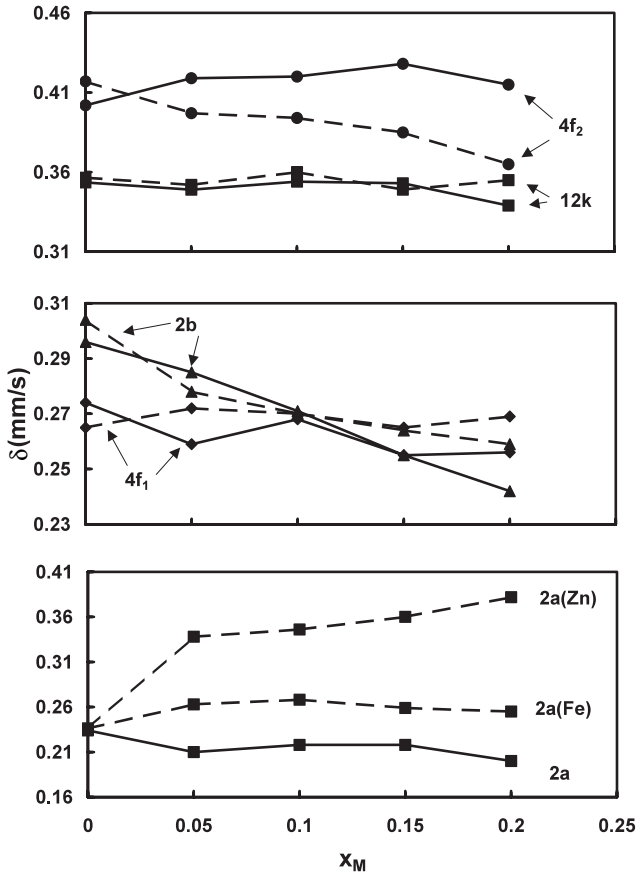

Figure 13. Isomer shift (relative to metallic iron) of the different contributions used to fit the Mössbauer spectrum of the M-type phase. The continuous and dotted lines correspond to the La–Co and La–Zn powders, respectively. The experimental errors are ±0.01, ±0.02, ±0.02, ±0.04 and ±0.03 mm s^{-1}, for the 12k, $4f_1$, $4f_2$, 2a and 2b contributions, respectively.

3.2.4. Discussion The evolution of the hyperfine parameters of the different contributions to the Mössbauer spectrum of the M-type phase in La–Zn and La–Co substituted ferrites can be interpreted in terms of the location of La^{3+}, Zn^{2+} and Co^{2+} ions in the M-type structure. The M-type structure and the surroundings of five Fe^{3+} sites are shown in figure 10. The number of nearest Fe^{3+} and Sr^{2+} neighbours and the corresponding mean distances [7, 30] for each Fe^{3+} site in the crystal structure of the M-type phase in $SrFe_{12}O_{19}$ are reported in table 2.

Because the $4f_2$ and 2b sites have three Sr^{2+} ions in their vicinity, the substitution of Sr^{2+} ions by La^{3+} ions induces a perturbation of both the symmetry and the charge density around these sites. The Sr^{2+} site being closer to the 2b site (the corresponding distance is $d = 0.340$ nm) than to the $4f_2$ site (the corresponding distance is $d = 0.366$ nm), the perturbation caused by the presence of La^{3+} ions in the Sr^{2+} sites is strongest for the 2b sites than for the $4f_2$ sites. This leads to important changes of the hyperfine parameters of the 2b contribution as detected by Mössbauer spectrometry. The Sr^{2+}/La^{3+} substitution induces a perturbation of the symmetry around the 2b and $4f_2$ sites, which is responsible for the changes of the quadrupolar shift observed both in La–Co and La–Zn samples. In particular, it makes the oxygen bipyramid of the 2b site more symmetric [31], resulting in an important decrease of the quadrupolar shift of

Table 2. Number of nearest Fe^{3+} and Sr^{2+} neighbours and corresponding mean distances for each Fe^{3+} site in the crystal structure of the M-type phase in $SrFe_{12}O_{19}$ (after [7, 30]).

Site	12k	$4f_1$	$4f_2$	2a	2b	Sr
12k	4	3	2	1	1	1
	0.290 nm	0.357 nm	0.349 nm	0.305 nm	0.377 nm	0.365 nm
$4f_1$	9	3	—	3	—	—
	0.357 nm	0.362 nm		0.345 nm		
$4f_2$	6	—	1	—	3	3
	0.349 nm		0.272 nm		0.366 nm	0.366 nm
2a	6	6	—	—	—	—
	0.305 nm	0.345 nm				
2b	6	—	6	—	—	3
	0.377 nm		0.366 nm			0.340 nm

the corresponding Mössbauer contribution. The isomer shift of the 2b contribution decreases for both series of samples, indicating an increase of the electron density in the vicinity of the 2b site. A similar trend has already been observed for $BaFe_{12}O_{19}$ ferrites when Ba^{2+} ions are replaced by La^{3+} ions [31]. The decrease of the isomer shift of the 2b contribution is thus attributed to an increase of the number of La^{3+} ions in the vicinity of the 2b site.

On the other hand, a decrease of the isomer shift of the $4f_2$ contribution is observed for the La–Zn samples. Such a decrease is not observed for the La–Co samples, and this can be interpreted by considering the influence of the Fe^{3+}/Co^{2+} substitution in the $4f_2$ sites, where a $4f_2$ site has one $4f_2$ neighbour (see figure 10) in its close vicinity ($d = 0.272$ nm). In La–Co samples, a simultaneous substitution of Sr^{2+} by La^{3+} and of Fe^{3+} by Co^{2+} (in the $4f_2$ sites) occurs, with the same proportions. This induces a compensation for the lack of negative charge (due to the Sr^{2+}/La^{3+} substitution) by an excess of negative charge (due to the Fe^{3+}/Co^{2+} substitution), and the isomer shift of the $4f_2$ contribution remains constant when the experimental errors are taken into account. In the La–Zn samples, the Zn^{2+} ions are present in the $4f_1$ sites and not in the $4f_2$ sites. As the $4f_2$ site has no $4f_1$ neighbour, the charge compensation does not occur in the La–Zn samples and the isomer shift of the $4f_2$ contribution decreases, as for the 2b contribution. It is worth mentioning that, in $Sr_{1-x}La_xFe_{12-y}Co_yO_{19}$ ($y < x$) powders where the M-type phase contains more La^{3+} than Co^{2+}, the charge compensation does not occur, and this explains the observed decrease of the isomer shift of the $4f_2$ Mössbauer contribution [29].

Because the 12k, $4f_1$ and 2a sites have $4f_1$ sites in their vicinity (see table 2 and figure 10), the substitution of Fe^{3+} ions by the non-magnetic Zn^{2+} ions in the $4f_1$ site induces a perturbation of the superexchange 12k–O^{2-}–$4f_1$, $4f_1$–O^{2-}–$4f_1$ and 2a–O^{2-}–$4f_1$ interactions. As x_M increases, the increase of the number of Zn^{2+} ions in the vicinity of the 12k, $4f_1$ and 2a sites in La–Zn substituted samples leads to a decrease of the hyperfine fields of the corresponding contributions, as observed by Mössbauer spectrometry. As the $4f_2$ site has no $4f_1$ neighbour in its close vicinity, the Fe^{3+}/Zn^{2+} substitution in the $4f_1$ site does not influence the hyperfine field of the $4f_2$ contribution. The weak decrease of the hyperfine field of the $4f_2$ contribution can be attributed to the Sr^{2+}/La^{3+} substitution, or to the perturbation of the hyperfine field at the 12k and 2b sites, or both. The substitution of a magnetic trivalent ion by a non-magnetic divalent ion in the $4f_1$ site and the fact that the $4f_1$ site is in the vicinity of three 2a sites cause an important perturbation of both symmetry and electron density around the 2a site. This explains the important modifications of the hyperfine parameters of the 2a(Fe) and 2a(Zn) contributions observed in the La–Zn substituted ferrites.

Because the 12k and $4f_2$ sites have $4f_2$ sites in their vicinity (see table 2 and figure 10), the substitution of Fe^{3+} ions by Co^{2+} magnetic ions in the $4f_2$ site induces a perturbation of the superexchange 12k–O^{2-}–$4f_2$ and $4f_2$–O^{2-}–$4f_2$ interactions. On the other hand, as the 12k and $4f_1$ sites have 2a sites in their vicinity, the substitution of Fe^{3+} ions by Co^{2+} ions in the 2a site induces a perturbation of the superexchange 12k–O^{2-}–2a and $4f_1$–O^{2-}–2a interactions. Consequently, this double substitution leads to variations of the hyperfine field of the 12k, $4f_1$ and $4f_2$ contributions. However, these variations are weaker than those in the La–Zn samples because the Co^{2+} ion is magnetic. The superexchange 2b–O^{2-}–$4f_2$ interactions are also perturbed by the Fe^{3+}/Co^{2+} substitution in the $4f_2$ site. However, as Co^{2+} is magnetic, this perturbation is probably weak and the changes of the hyperfine parameters of the 2b contribution detected by Mössbauer spectrometry are attributed mainly to Sr^{2+}/La^{3+} substitution.

These results confirm unambiguously that La^{3+} ions are located in the Sr^{2+} sites; Zn^{2+} ions are located in the $4f_1$ sites and Co^{2+} ions are located in both $4f_2$ and 2a sites.

4. Conclusions

This investigation shows that it is possible to synthesize the M-type phase with $Sr_{1-x}La_xFe_{12-x}Zn_xO_{19}$ or $Sr_{1-x}La_xFe_{12-x}Co_xO_{19}$ composition ($x = 0.1, 0.2, 0.3, 0.4$) by chemical co-precipitation. However, the ultrafine powders are not single, hexagonal M-type phase, as they contain (La, Sr)FeO_3, $ZnFe_2O_4$ or $CoFe_2O_4$ secondary phases. For each sample, the Mössbauer relative intensity of all the secondary phases does not exceed 10% of the whole Mössbauer intensity. It is expected that the amount of secondary phases could be reduced by optimizing the processing parameters (calcination temperature and time). Due to the presence of La, Zn and Co containing secondary phases, the La, Zn and Co content in the M-type phase is lower than that corresponding to the nominal values. However, the M-type phase contains La^{3+} and Zn^{2+}, or La^{3+} and Co^{2+} in the same proportions.

A complete Mössbauer analysis of the substitution effects in the M-type phase was carried out by means of a comparison between the spectra of the La–Zn and La–Co substituted samples. The evolution with x of the hyperfine parameters of the components used to fit the contribution of the M-type phase have been interpreted consistently in terms of the substitution effects, in both La–Zn and La–Co samples. The results show unambiguously that, La^{3+} ions are located in the Sr^{2+} sites, Zn^{2+} ions are located in the $4f_1$ sites and Co^{2+} ions are located in both the $4f_2$ and 2a sites. This is consistent with the results obtained for La–Zn and La–Co substituted samples prepared according to a conventional ceramic process, and shows that the location of the Zn^{2+} and Co^{2+} ions in the M-type structure does not depend on the particular synthesis method.

As Zn^{2+} and Co^{2+} ions are located in different sites, the replacement of some Fe^{3+} ions by non-magnetic Zn^{2+} ions in the antiparallel $4f_1$ sites in $Sr_{1-x}La_xFe_{12-x}Co_xO_{19}$ ferrites should lead to an increase of the magnetization of the M-type phase. Such an investigation is in progress.

Acknowledgments

The authors would like to thank Dr A Morel (Carbone Lorraine Ferrites, Evreux) for providing the $Sr_{0.7}La_{0.3}Fe_{11.7}Zn_{0.3}O_{19}$ powder made by a ceramic process.

References

[1] Taguchi H, Takeishi T, Suwa K, Masuzawa K and Minachi Y 1996 *Proc. 7th Int. Conf. on Ferrites (Bordeaux, France, Sept. 1996)* ed V Cagan and M Guyot p C1-311
[2] Smolenskii G and Andreev A 1961 *Bull. Acad. Sci. USSR* **25** 1405
[3] Ida K, Minachi Y, Masuzawa K, Nishio H and Taguchi H 1999 *J. Mag. Soc. Japan* **23** 1093
[4] Taguchi H, Minachi Y, Masuzawa K and Nishio H 2000 *Proc. 8th Int. Conf. on Ferrites (Kyoto, Japan, Sept. 2000)* ed M Abe and Y Yamazaki p 405
[5] Kools F, Morel A, Tenaud P, Rossignol M, Isnard O, Grössinger R, Le Breton J M and Teillet J 2000 *Proc. 8th Int. Conf. on Ferrites (Kyoto, Japan, Sept. 2000)* ed M Abe and Y Yamazaki p 437
[6] Gorter E W 1954 *Philips Res. Rep.* **9** 403
[7] Wartewig P, Krauze M K, Esquinazi P, Rösler S and Sonntag R 1999 *J. Magn. Magn. Mater.* **192** 83
[8] Miller S 1959 *J. Appl. Phys.* **30** 245
[9] Mulay V N and Sinha A P B 1970 *Indian J. Pure Appl. Phys.* **8** 412
[10] Le Breton J M, Wiesinger G, Tellez Blanco C, Isnard O, Teillet J, Grössinger R, Morel A, Kools F and Tenaud P 2000 *Proc. 8th Int. Conf. on Ferrites (Kyoto, Japan, Sept. 2000)* ed M Abe and Y Yamazaki p 199
[11] Kamb B 1968 *Am. Mineral.* **53** 1439
[12] Morel A, Le Breton J M, Kreisel J, Wiesinger G, Kools F and Tenaud P 2002 *J. Magn. Magn. Mater.* **242–245** 1405
[13] Le Breton J M, Teillet J, Wiesinger G, Morel A, Kools F and Tenaud P 2002 *IEEE Trans. Magn.* **38** 2952
[14] Pieper M, Morel A and Kools F 2002 *Phys. Rev.* B **65** 184402
[15] Wang J F, Ponton C B and Harris I R 2001 *J. Magn. Magn. Mater.* **234** 233
[16] Wang J F, Ponton C B and Harris I R 2002 *IEEE Trans. Magn.* **38** 2928
[17] Teillet J and Varret F 1983 *MOSFIT Program* unpublished
[18] Mocuta H, Lechevallier L, Le Breton J M, Wang J F and Harris I R 2003 *J. Alloys Compounds* **364** 48
[19] Uhm Y R, Sur J C and Kim C S 2000 *J. Magn. Magn. Mater.* **215** 554
[20] Eibschütz M, Shtrikman S and Trevers D 1967 *Phys. Rev.* **156** 562
[21] Sepelak V, Wißmann S and Becker K D 1999 *J. Magn. Magn. Mater.* **203** 135
[22] Burghart F J, Potzel W, Kalvius G M, Schreier E, Grosse G, Noakes D R, Schäfer W, Kockelmann W, Campbell S J, Kaczmarek W A, Martin A and Krause M K 2000 *Physica* B **289** 286
[23] Grigorova M, Blythe H J, Blaskov V, Rusanov V, Petkov V, Masheva V, Nihtianova D, Martinez L M, Muñoz J S and Mikhov M 1998 *J. Magn. Magn. Mater.* **183** 163
[24] Kim S J, Lee S W, An S Y and Kim C S 2000 *J. Magn. Magn. Mater.* **215** 210
[25] Van Diepen A M and Lotgering F K 1974 *J. Phys. Chem. Solids* **35** 1641
[26] Albanese G 1995 *J. Magn. Magn. Mater.* **147** 421
[27] Rensen J G, Schulkes J A and van Wieringen J S 1971 *J. Physique Coll.* **32** C1 924
[28] Evans B J, Grandjean F, Lilot A P, Vogel R H and Gerard A 1987 *J. Magn. Magn. Mater.* **67** 123
[29] Lechevallier L, Le Breton J M, Teillet J, Morel A, Kools F and Tenaud P 2003 *Physica* B **327** 135
[30] Obradors X, Solans X, Collomb A, Samaras D, Rodriguez J, Pernet M and Font-Altaba M 1988 *J. Solid State Chem.* **72** 218
[31] Sauer Ch, Köbler U, Zinn W and Stäblein H 1978 *J. Phys. Chem. Solids* **39** 1197